analytical chemistry

Article

pubs.acs.org/ac

Cluster Secondary Ion Mass Spectrometry and the Temperature Dependence of Molecular Depth Profiles

Dan Mao,[†] Andreas Wucher,[‡] Daniel A. Brenes,[†] Caiyan Lu,[†] and Nicholas Winograd*,[†]

[†]The Pennsylvania State University, Department of Chemistry, University Park, Pennsylvania 16802, United States

[‡]Faculty of Physics, University of Duisburg-Essen, 47048 Duisburg, Germany

ABSTRACT: The quality of molecular depth profiles created by erosion of organic materials by cluster ion beams exhibits a strong dependence upon temperature. To elucidate the fundamental nature of this dependence, we employ the Irganox 3114/1010 organic delta-layer reference material as a model system. This delta-layer system is interrogated using a 40 keV C_{60}^+ primary ion beam. Parameters associated with the depth profile such as depth resolution, uniformity of sputtering yield, and topography are evaluated between 90 and 300 K using a unique wedge-crater beveling strategy that allows these parameters to be determined as a function of erosion depth from atomic force microscope (AFM) measurements. The results show that the erosion rate calibration performed using the known Δ-layer depth in connection with the fluence needed to reach the peak of the corresponding secondary ion mass spectrometry (SIMS) signal response is misleading. Moreover, we show that the degradation of depth resolution is linked to a decrease of the average erosion rate and the buildup of surface topography in a thermally activated manner. This underlying process starts to influence the depth profile above a threshold temperature between 210 and 250 K for the system studied here. Below that threshold, the process is inhibited and steady-state conditions are reached with constant erosion rate, depth resolution, and molecular secondary ion signals from both the matrix and the Δ-layers. In particular, the results indicate that further reduction of the temperature below 90 K does not lead to further improvement of the depth profile. Above the threshold, the process becomes stronger at higher temperature, leading to an immediate decrease of the molecular secondary ion signals. This signal decay is most pronounced for the highest m/z ions but is less for the smaller m/z ions, indicating a shift toward small fragments by accumulation of chemical damage. The erosion rate decay and surface roughness buildup, on the other hand, exhibit a rather sudden delayed onset after erosion of about 150 nm, indicating that a certain damage level must be reached in order to influence the erosion dynamics. Only after that onset does the depth resolution become compromised, indicating that the temperature reduction does not significantly influence parameters like ion-beam mixing or the altered-layer thickness. In general, the wedge-crater beveling protocol is shown to provide a powerful basis for increased understanding of the fundamental factors that affect the important parameters associated with molecular depth profiling.

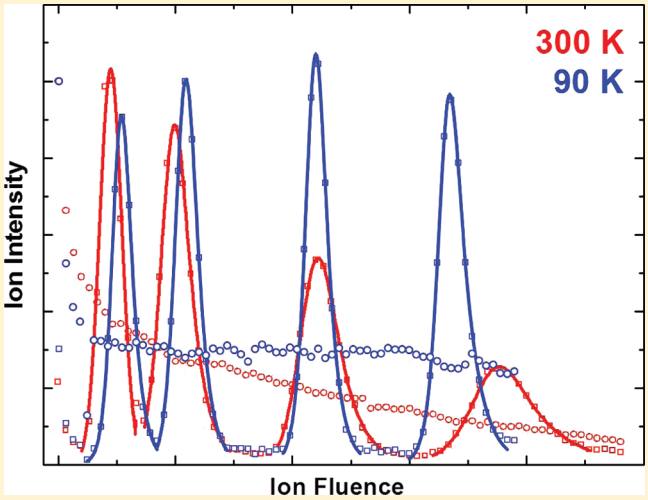

Molecular depth profiling of organic and biological materials using secondary ion mass spectrometry (SIMS) and cluster ion beams has rapidly emerged as an important novel tool for the characterization of complex multilayer systems.[1−10] With this method, molecular and fragment distribution information as a function of depth is acquired by erosion of the sample with energetic cluster ion beams, typically consisting of SF_5^+, C_{60}^+ ,or Ar_x^+ clusters with x up to 10 000.[6,11−17] In addition, since 2-dimensional images can be recorded as a function of eroded depth, it is possible to create a molecule-specific 3-dimensional rendering of the material by a simple stacking of these images.[18−23] Fundamental studies have been reported recently which describe experimental conditions that yield minimal chemical damage accumulation during erosion, maximum depth resolution, and minimal topography buildup. The most promising approaches include using larger cluster ion sources, such as argon clusters,[24,25] sputtering at glancing angles,[9,26] cooling of the sample to <100 K,[5,8,9] and rotation of the sample stage.[8,10]

There are often compromises when attempting these optimization strategies. For example, sample rotation during a depth profile improves depth resolution from an initially flat surface but is problematic for irregularly shaped objects. Sputtering at a glancing angle is believed to minimize interlayer mixing induced by bombardment as it significantly reduces the

Received: December 8, 2011
Accepted: March 27, 2012
Published: March 27, 2012

   dx.doi.org/10.1021/ac2032589 | *Anal. Chem.* 2012, 84, 3981−3989

trailing edge of the depth profiling peaks,[9] but sputtering yield and spatial resolution are degraded. Bombardment with Ar_x^+ clusters has been shown to improve depth resolution and reduce chemical damage.[7] So far, however, these sources cannot be focused to a submicrometer spot size for high resolution imaging; the SIMS ion yields are somewhat reduced over other projectiles, and the sputtering yield is not as high, especially for the largest cluster projectiles.[17]

Reduced temperature has been shown to yield reduced chemical damage and topography.[5,9] Coincidentally, sample cooling has also been widely used for biological applications of SIMS since sample integrity is maintained and cellular information in a hydrated frozen state prevents the collapse of cells in a high vacuum environment.[27−29] Sample cooling has been shown to reduce chemical damage accumulation for other organic systems including poly (methyl methacrylate) (PMMA),[30] Langmuir−Blodgett (LB) multilayered thin films,[5,9] and Irganox multilayered thin films.[8,31] The reason behind this observation is not clear, and there are, as yet, no general guidelines for employing low temperature experiments in concert with the other parameters known to improve depth profiling. For example, it is not known whether temperature is responsible for abruptly or gradually turning off the damage accumulation, how topography formation changes with temperature, and whether there is an optimal temperature value which optimizes depth resolution.[5,8,9]

Here, we examine the influence of temperature in detail by a combination of conventional sputter depth profiling, wedge-crater beveling, and atomic force microscopy (AFM). A major advantage of wedge-crater beveling is that all factors regarding depth profiling including interface widths, topography, and sputtering yield can be obtained at every point in the depth profile from a single crater measurement. An organic multilayered system of Irganox 3114/1010 is employed as a model for this investigation. This sample is prepared as a standard reference material by the National Physical Laboratory in the U.K. and has been the subject of a round-robin analysis involving more than 20 different groups.[3,7,8,10] The goal is to acquire and characterize depth profiles of the buried Irganox 3114 Δ-layers as a function of sample temperature, ranging from 90 to 300 K. Results of conventional depth profiles are compared to those obtained with the wedge-shaped crater beveling technique using a focused 40 keV C_{60}^+ ion beam for sample erosion and SIMS data acquisition.

Depth profile data are complemented with AFM measurements of the eroded crater, which in combination with the wedge beveling technique provide extremely valuable additional information regarding the dynamics of erosion rate and the emergence of surface roughness. Depth profiles are acquired in the imaging mode, either as a series of mass spectral images separated by homogeneous erosion cycles for conventional depth profiling or by acquisition of one single image of the wedge-shaped sputter crater. The results show that erosion rate decay and surface roughening are linked and start to occur abruptly at a certain eroded depth. Both effects are prominent at sample temperatures of 250 K and above, where they keep growing in magnitude with increasing sputtered depth, but can be effectively suppressed if the sample temperature is lowered below 250 K. The results also reveal a degradation of the secondary ion yield which appears to be much more pronounced than the erosion rate decay and is even observed when the erosion rate is maintained throughout the depth profile.

EXPERIMENTAL SECTION

Materials and Samples. An organic Δ-layer system was constructed by the National Physical Laboratory (NPL) using Irganox 1010 and Irganox 3114 as described previously.[3] Thin marker layers of Irganox 3114 (∼0.9 nm) were deposited between thick layers of Irganox 1010 (∼47.1 nm or ∼94.3 nm), resulting in a Δ-layer structure which is ideally suited to investigate depth resolution in a similar fashion to that routinely carried out for inorganic depth profiling.[32] The film thicknesses of each layer from surface to substrate are listed in Table 1.

Table 1. Structure of Irganox 1010/3114 Δ-Layer Samples (1 nm) Manufactured by NPL[a]

layer	type	sample (nm)
1	Irganox 1010	47.1
2	Irganox 3114	0.9
3	Irganox 1010	47.1
4	Irganox 3114	0.9
5	Irganox 1010	94.3
6	Irganox 3114	0.9
7	Irganox 1010	94.2
8	Irganox 3114	0.9
9	Irganox 1010	94.2

[a]Four Irganox 3114 Δ-layers of 0.9 nm are embedded into an Irganox 1010 matrix film (approximately 380 nm) deposited on a silicon substrate covered with silicon dioxide.

Instrumentation. Depth profiling was performed in a TOF-SIMS instrument equipped with a C_{60} cluster ion source (IOG 40-60, Ionoptika; Southampton, U.K.), directed at a 40° angle relative to the surface normal. The performance of the C_{60} ion source and details of this instrumentation have been described elsewhere.[11,33] For conventional depth profiling experiments, the 40 keV C_{60}^+ ion beam was operated alternatively between data acquisition and material sputtering cycles. A continuous ("dc") beam of measured current of ∼80 pA into a spot size of ∼10 μm was used to erode a 190 μm × 250 μm area of the film with removal of 4−5 nm of material per interval. For conventional depth profiling, a stable primary ion beam current is crucial because AFM data can be measured only from the completely eroded crater. Current measurements were taken before and after erosion of each crater to ensure the stability of the ion beam.

The wedge sputter depth profiling scheme has been described previously.[34] Briefly, the surface is subjected to one or two erosion cycles with the 40 keV C_{60}^+ ion beam operated in dc mode and digitally scanned across a 460 μm × 600 μm field of view using a 256 × 256 pixel raster. The total scanning time of each cycle is divided into frames with a beam dwell time of about 20 μs on each pixel. In order to erode a wedge-shaped crater, a linearly increasing ion fluence is applied which varies between zero on one side of the crater to a maximum value on the other side. For that purpose, the raster area is varied from frame to frame by sequentially skipping more and more lines in the *y*-direction, beginning with the line closest to the ion source.

The TOF-SIMS instrument used in these experiments has the capability of sample cooling by forcing liquid-nitrogen-cooled N_2 gas through the sample stage. Because the stage is pulsed to a high voltage potential during the SIMS analysis, a direct measurement of the sample temperature is not possible

dx.doi.org/10.1021/ac2032589 | Anal. Chem. 2012, 84, 3981−3989

during data acquisition. Temperature readings were collected using a thermocouple wired to the stage before and after each experiment. A constant flow of N_2 gas is first established through a copper tube imbedded into liquid nitrogen. Under normal operating conditions, the N_2 gas is at least partly condensed into a liquid nitrogen flow through the sample stage, resulting in a stable stage temperature of ~90 K. In order to stabilize the temperature at higher values between 90 and 300 K, a heater is wrapped around the copper tube and operated at a fixed electrical power. By balancing the N_2 line gas flow and the heating power, a stable stage temperature is obtained within ~1 h which then remains constant within ±5 K for the duration of the experiment.

For conventional image depth profiling, negative ion SIMS images were taken from the center area of about 115 μm × 150 μm within the erosion area (190 μm × 250 μm) between subsequent erosion cycles. For wedge-crater beveling depth profiling, SIMS images of the eroded wedge-shaped crater were taken from an analysis field of view of 520 μm × 675 μm when the largest erosion depth reached ~150 and ~400 nm, respectively. In the latter case, the entire film is removed at the deep side of the eroded crater. SIMS images were acquired using the pulsed C_{60}^+ beam (pulse width 50 ns) digitally rastered across a pattern of 256 × 256 pixels. AFM characterization of the eroded craters was performed using a KLA-Tencor Nanopics 2100 wide area AFM. For the analysis of the wedge-shaped craters, the AFM images were taken at 800 μm × 800 μm field of view in order to enclose the entire crater into one image. The data were taken in contact mode, but it was checked that images taken in damping (tapping) mode delivered the same information. Extreme care was taken to process the AFM results, minimizing the instrumentation artifacts of the topography information on the wedge surface.

RESULTS AND DISCUSSION

In previous work, we have shown that, by combining topographical information from AFM with SIMS in a beveled crater, direct information about surface roughness, erosion rate, and depth resolution can be obtained from a single measurement. The protocol necessary to extract this information from topographical line scans along the wedge direction (y-) of the eroded crater has been described previously.[34] Briefly, the process utilizes the fact that there is a linear relationship between the y-coordinate along the line scan and the ion fluence. The erosion rate can therefore be directly calculated from the average slope of the (smoothed) wedge crater surface and evaluated as a function of depth from a single crater profile. Microscopic fluctuations of the surface height, on the other hand, reflect the surface roughness, which can be obtained by subtracting the original AFM line scan from smoothed data. At the same time, the depth resolution can be obtained by determining the full width at half maximum (fwhm) of the SIMS signal characteristic of the Irganox 3114 Δ-layer when plotted along the same line scan across the SIMS image of the crater bottom after calibration of the depth scale using AFM.

In previous work, all of the important parameters used to describe a depth profile were significantly improved when reducing the temperature from 300 to 90 K.[31] The purpose of this work is to further investigate the cause of that effect by varying the sample temperature between these two extremes. Conventional sputter depth profiles measured at four different sample temperatures of 90, 150, 250, and 300 K are shown in Figure 1. The signal of the largest Irganox 3114 specific fragment at m/z 564 ($C_{33}H_{46}N_3O_5^-$) and a relatively small fragment at m/z 42(CNO^-) are plotted versus the C_{60}^+ ion fluence. The matrix signal, corresponding to the Irganox 1010 specific fragment at m/z 59 ($C_2H_3O_2^-$), is also included for reference purposes. In accordance with previously published data, several observations are evident from the figure: (i) the secondary ion signals representing the Irganox 3114 Δ-layers track each other, (ii) the signals representing both the Irganox 1010 matrix and the Irganox 3114 Δ-layers decrease with increasing eroded depth, and (iii) the apparent fwhm of the Δ-layer increases with increasing eroded depth.

Effects (ii) and (iii) are most pronounced if the depth profile is performed at 300 K and agree with similar findings published earlier.[3,8] These effects have been attributed to a degradation of the depth resolution which is assumed to be caused by increased surface roughness built up during ion bombardment.[3] However, if the signal representing the Δ-layer is integrated over the entire response peak, the resulting signal is still found to decrease at 300 K as shown in Table 2. Hence, other factors in addition to the degraded depth resolution must contribute to the observed signal decay. Moreover, it has been proposed that the average erosion rate between subsequent Δ-layers can be determined from their known depths and the fluence interval needed to reach the corresponding peak in the SIMS signal. Data obtained using this strategy is shown in Figure 2, using the depth values of 48, 96, 192, and 288 nm for the first, second, third, and fourth Δ-layer as given by the manufacturer. The data indicate a decrease of the average erosion rate with increasing eroded depth, which appears to be most pronounced at the highest temperature and is practically absent at temperatures below 150 K. The fact that the calculated erosion rate at 150 K appears to be slightly larger than that calculated at 90 K is probably due to uncertainty of the C_{60} projectile ion current measurement.

In principle, the depth resolution can be calculated from the fwhm of the Δ-layer peaks and the known depth interval between subsequent Δ-layers. The results obtained in this way are also shown for all four Δ-layers in Table 2. It is interesting that the depth resolution for the first Δ-layer is virtually identical for all four investigated temperatures. This observation indicates that there is no change in critical parameters like ion beam mixing or the information depth by reducing the sample temperature. For the deeper Δ-layers, however, reduced sample temperature helps to maintain the achieved depth resolution. This issue is discussed below in detail.

It is logical to assume that the degradation of the measured secondary ion signal, the depth resolution, and the erosion rate are connected and caused by chemical damage in the molecular film building up and accumulating under prolonged ion bombardment. To investigate this notion further, one can trace the SIMS signals of the molecular ion and characteristic fragments of the Irganox 1010 matrix as shown in Figure 3. The measured ion intensities have been normalized to their respective value obtained in the first spectrum at the beginning of the depth profile. In order to illustrate the trends, the data have been plotted only for the highest and lowest sample temperature studied here. As is visible for the m/z 59 fragment in Figure 1, the data obtained at 150 K look similar to those obtained at 90 K, while those obtained at 250 K resemble those measured at 300 K, albeit with a significantly less pronounced decay. As seen from Table 2, the same trends are observed for the integrated Δ-layer signals as well. It is immediately evident that the two cases are largely different. At the beginning of the

dx.doi.org/10.1021/ac2032589 | Anal. Chem. 2012, 84, 3981−3989

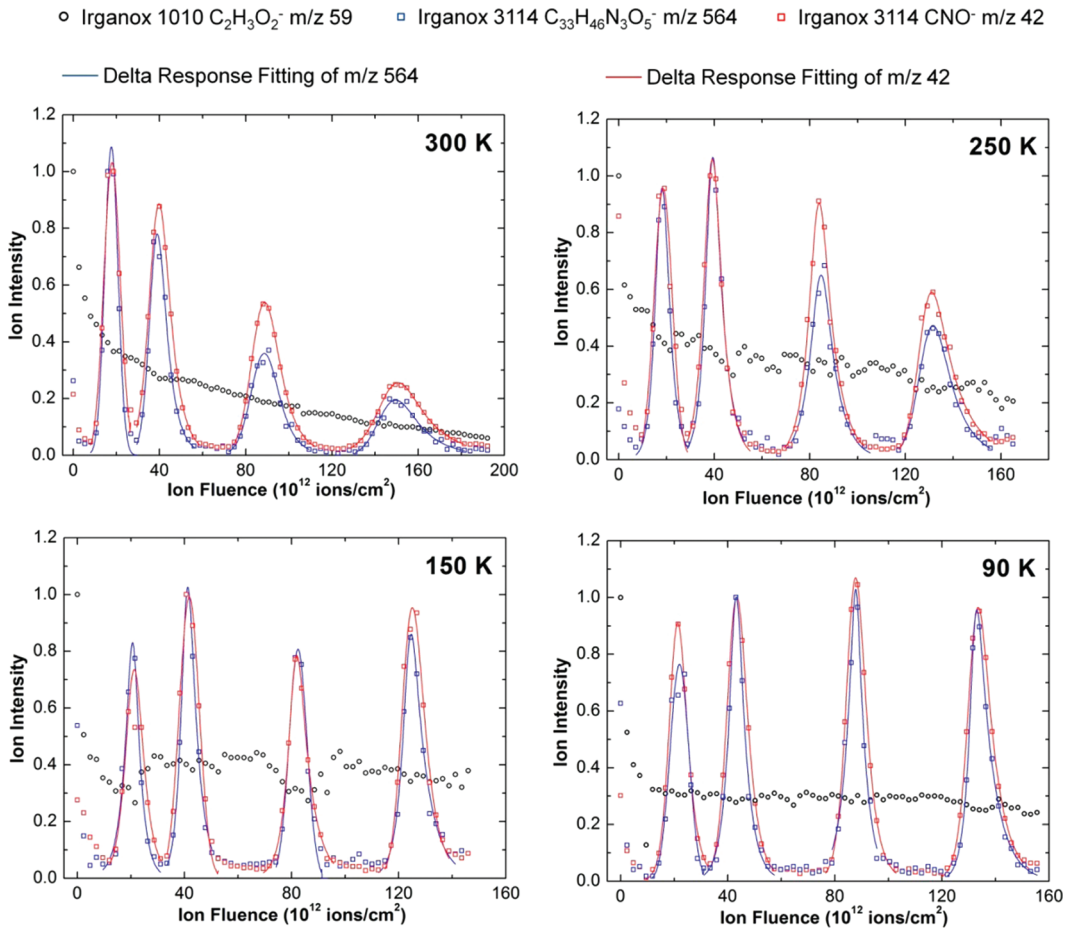

Figure 1. Conventional sputter depth profiles of Irganox 1010/3114 multilayer sample at 300, 250, 150, and 90 K with C_{60}^+ incident at 40° with respect to the surface normal. The Irganox 1010 matrix signal ($C_2H_3O_2^-$ m/z 59) is normalized to surface intensity, and the Irganox 3114 Δ-layer signals ($C_{33}H_{46}N_3O_5^-$ m/z 564, CNO^- m/z 42) are normalized to their maximum intensity during the entire depth profile.

Table 2. Depth Resolution and Integrated SIMS Signal of the m/z 564 Fragment Measured for Δ-Layers during Depth Profiles Obtained at 300, 250, 150, and 90 K as Shown in Figure 1[a]

temperature (K)		300	250	150	90
1st layer	fwhm (nm)	14	15	13	15
	signal	1.0	1.0	1.0	1.0
2nd layer	fwhm (nm)	19	17	13	14
	signal	1.0	1.3	1.2	1.2
3rd layer	fwhm (nm)	25	20	15	14
	signal	0.7	1.1	1.4	1.2
4th layer	fwhm (nm)	33	27	15	16
	signal	0.6	1.1	1.1	1.4

[a]The 3rd and 4th Δ-layer values are estimated assuming a constant erosion rate decay and are therefore only approximate values. The estimated error of the measured depth resolution is ±1 nm. The integrated signal is calculated from the Dowsett fitting curves of each peak and normalized to that of the 1st layer.

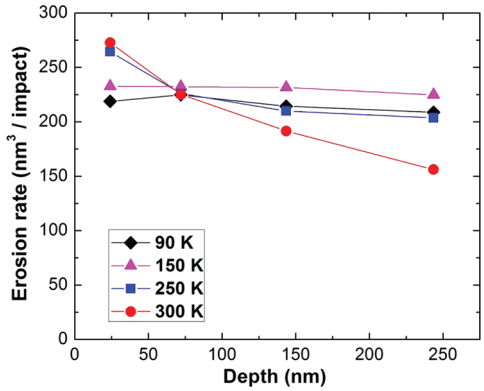

Figure 2. Erosion rate calculated from conventional depth profiles by dividing the known depth of each delta layer by the ion fluence needed to reach the peak signal corresponding to this layer.

depth profile, all signals exhibit a relatively rapid decay during the fluence interval up to 1×10^{13} ions/cm^2. This behavior is well-known and indicates the onset of ion beam induced fragmentation as described by the erosion dynamics model.[35]

The magnitude of the decay is most pronounced for the molecular ion and decreases with decreasing fragment size, indicating a larger damage cross section for the molecular ion. At 90 K, all signals reach a steady state after this initial decay, indicating a stable balance between ion beam induced damage/fragmentation and sputter removal, the latter being characterized by a stable sputter yield or erosion rate. At 300 K, on the other hand, all signals continue to decay with increasing fluence, yet at a slower rate, which is largest for the molecular ion and decreases with decreasing fragment size. The fact that smaller fragments decrease faster than larger ones indicates a shift toward smaller fragments in the spectrum and is therefore indicative of accumulating ion beam induced chemical damage. One additional observation in Figure 1 is that when there is no

dx.doi.org/10.1021/ac2032589 | Anal. Chem. 2012, 84, 3981−3989

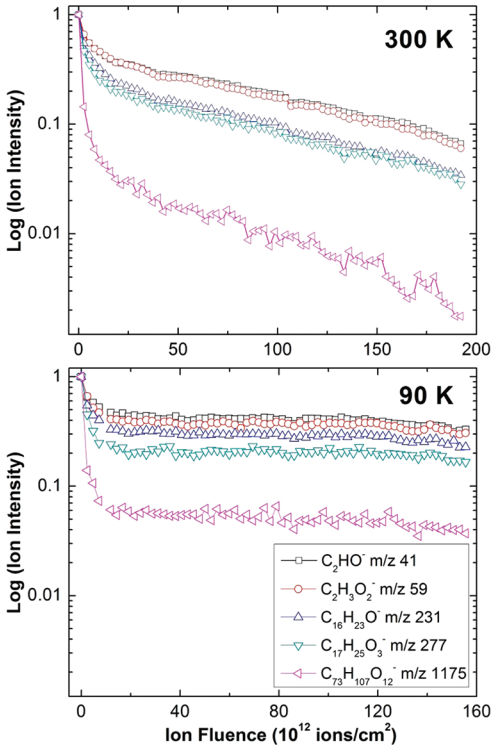

Figure 3. Depth profiles of different Irganox 1010 matrix signals at 300 K (top panel) and 90 K (lower panel) with 40-keV C_{60}^+ at 40° incident angle. Each fragment signal is normalized to its surface intensity.

signal decay there is no difference between the behavior of big and small fragments, indicating that a stable damage level has been reached. As suggested by the erosion dynamics model, such a "quasi steady state" behavior should be indicative of a decreasing sputter yield,[3,36,37] a notion which appears to be in principle accordance with the data shown in Figure 1.

To investigate these points in more detail and complement the information presented in Figure 1, additional depth profiles were obtained using the wedge-shaped crater beveling technique at six different temperature points including 90, 130, 160, 210, 250, and 300 K. The wedge methodology was used because it allows information on erosion rates and surface roughness to be directly extracted. The results obtained as a function of temperature are discussed in the following sections.

Surface Roughening Effects. For surface roughness evaluation, the microscopic height fluctuations from the AFM data measured on the wedge-shaped erosion crater can be visually compared. To eliminate the macroscopic depth variations, the AFM topography scan is first smoothed by a 36-point Savitzky-Golay algorithm. The resulting curve represents the average height of the surface as a function of a linearly increasing ion fluence, the latter being represented by the length coordinate along the AFM line scan of the crater bottom. By subtracting this curve from the original AFM data, the microscopic height fluctuations representing the surface roughness can be obtained. The results of AFM line scans and the calculated height fluctuations are shown in Figure 4.

The height fluctuations can be categorized into three groups that are related to the sample temperature. At low temperature (upper panel of Figure 4), the height fluctuations remain constantly low during the removal of the entire film and are estimated to be around ±2.5 nm for the maximum peaks, with only minimal differences between 90 and 130 K. At intermediate temperatures (middle panels of Figure 4), the height fluctuations continue to remain constant throughout the entire wedge surface with no obvious increase as a function of ion fluence. However, the resulting curves fluctuate more intensely than at 90 K, with peak maxima around ±5 nm at 160 K and some even larger at 210 K. These results show that the surface roughening induced by ion bombardment is greater at these temperatures but stable, and the overall surface roughening is still minimal.

The third group consists of the profiles measured at 250 and 300 K (lower panels of Figure 4). In both cases, the height fluctuations start low at the initial surface and begin to increase at some point during the erosion process. The interesting observation is the relatively sudden onset of the roughening effect at an ion fluence corresponding to a total eroded depth of 150−200 nm. After this threshold, the surface roughness continues to build up until the entire film has been eroded. The maximum height fluctuations can be as large as ±10 nm and will therefore clearly influence the measured depth resolution. The data presented in Figure 4 nicely illustrate how the dynamics of the roughening process can be observed easily with a wedge shaped crater.

For a more quantitative assessment, the root-mean-square (rms) roughness value R_q is determined from the AFM data and compared for different sample temperatures. As described in detail elsewhere,[31] the momentary value of R_q at a specific point (i) in the line scan a is calculated as a running statistical average taken over 40 data points around (i) according to

$$R_q(i) = \sqrt{\frac{1}{2N}\sum_{k=i-N}^{i+N}[\Delta h(k)]^2} \quad (1)$$

using $N = 20$.

The R_q value determined in this way was averaged over intervals of 5 points ($i - 2$ to $i + 2$) and plotted as a function of eroded depth at point (i) in Figure 5. The error bars reflect the standard deviation of R_q within the respective 5-point interval. At all investigated temperatures, the roughness starts low at the beginning of the depth profile (i.e., the original surface) where R_q values are less than 2 nm. The roughness remains at this level during the entire crater erosion at both 90 and 130 K, with a little more fluctuation at 130 K. At 160 and 210 K, the roughness increases at an eroded depth around 150 nm but then stops increasing when reaching an R_q of about 2.5 nm. A stronger fluctuation is observed when the temperature increases, which suggests a bigger average surface roughening.

A fundamentally different behavior is observed at even larger sample temperatures. As seen in the lower panel of Figure 5, at 250 and 300 K, the roughness starts to rapidly increase at ∼150 nm and then continues to increase with eroded depth until the entire Irganox film is removed and the silicon substrate is reached, resulting in R_q larger than 4 nm. The overall increase of roughness throughout the depth profile is much greater when compared to lower sample temperatures. Note, however, that even at the largest investigated temperature, the roughness buildup is less than 5 nm, which is much smaller than the depth resolution degradation. Hence, depth resolution is not entirely limited to the surface roughening.

Overall, the surface topography data presented here show that lowering the sample temperature during ion bombardment inhibits the ion beam induced buildup of roughness on the

dx.doi.org/10.1021/ac2032589 | Anal. Chem. 2012, 84, 3981−3989

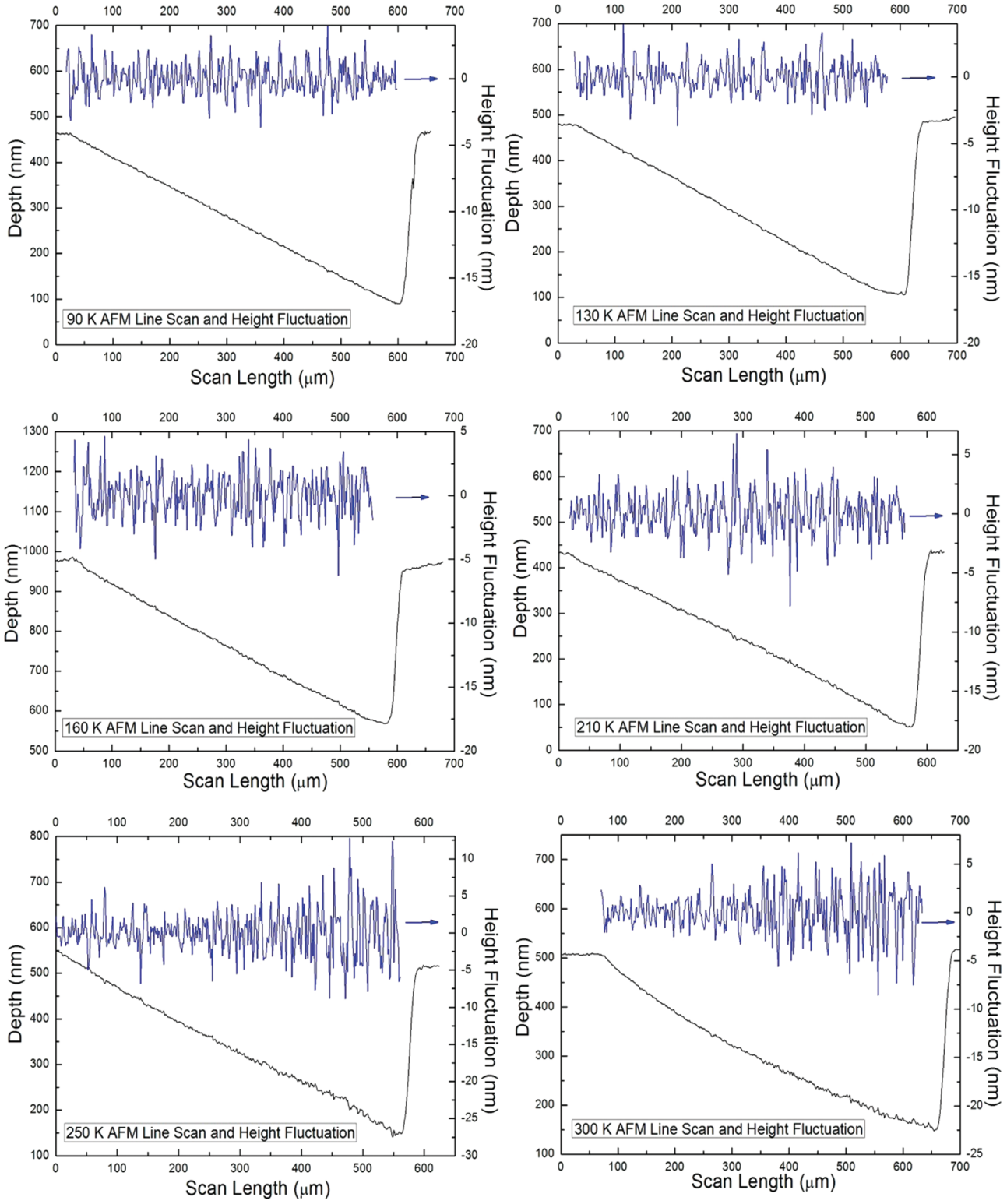

Figure 4. AFM topography scan along the wedge shaped craters eroded into a 380 nm thick Irganox 1010 film doped with four Irganox 3114 Δ-layers by a 40-keV C_{60}^+ ion beam impinging at 40° with respect to the surface normal at 90, 130, 160, 210, 250, and 300 K temperature. The blue curves represent the roughness fluctuations around the average crater profile calculated by subtracting the smoothed AFM scan data (black curves) from the original data.

sample surface. It should be noted that topography information as presented in Figure 5 would be extremely difficult to attain without the wedge beveling strategy. In a conventional depth profile, multiple craters must be eroded to multiple depths for subsequent AFM analysis for each single temperature, thereby greatly prolonging the data acquisition time. Moreover, each individual crater must naturally be eroded at a different lateral position, making the experiment sensitive to possible lateral inhomogeneities of the deposited molecular film.

Erosion Rate Decay Effects. The dynamics of the erosion rate as a function of the eroded depth can best be investigated using the wedge crater strategy. Since the surface receives a

dx.doi.org/10.1021/ac2032589 | *Anal. Chem.* 2012, 84, 3981−3989

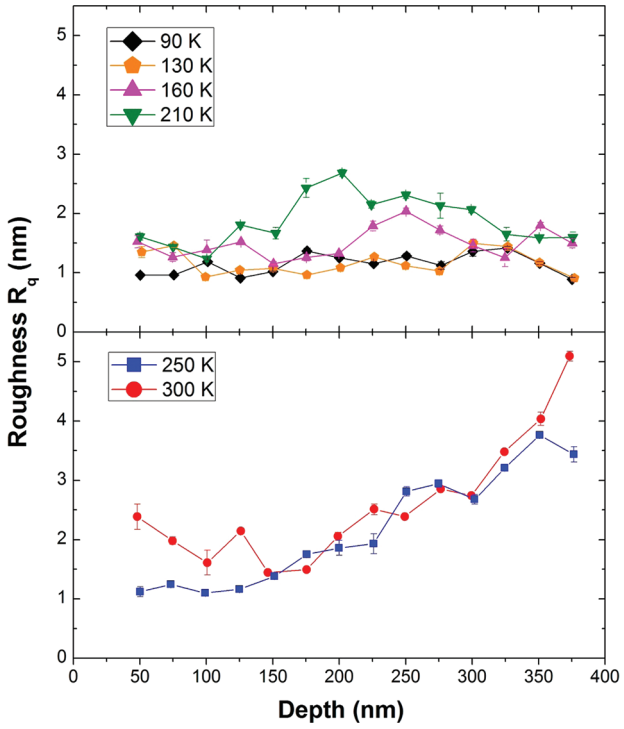

Figure 5. rms roughness (R_q value, see text) as a function of eroded depth during sputtering of the Irganox 1010/3114 Δ-layer film with a 40-keV C_{60}^+ ion beam impinging under 40° with respect to the surface normal. The data were obtained at six different sample temperatures during ion bombardment at 90, 130, 160, and 210 K (top panel) and 250 and 300 K (lower panel).

linearly increasing ion fluence along one direction of the raster area, line scans of the resulting surface topography along that direction directly reveal the fluence-depth relation. The erosion rate, defined as the eroded depth interval per unit ion fluence, is given by the derivative of that relation. It has the physical dimension of a volume and can be interpreted as the sputter yield volume, i.e., the average volume of sample removed per C_{60}^+ projectile ion impact. In conventional depth profiling, only the average erosion rate can be calculated from a single crater and many different craters would have to be eroded in order to obtain information about dynamic changes of this quantity. In a wedge crater, the advantage of having depth information at all ion fluences allows the determination of the erosion rate as a function of eroded depth, which is calculated in the form of a running numerical derivative of smoothed topographical AFM data as described previously.[34]

To eliminate residual microscopic fluctuations due to surface roughness and since we are only interested in macroscopic changes, the resulting erosion rate values were averaged over sets of 40 neighbored data points of the AFM line scan and plotted in Figure 6 at the depth corresponding to the center of each set. Again, the results will be discussed in two groups.

The first group consists of the experiments at 90, 130, 160, and 210 K as shown in the top panel of Figure 6. It is seen that for these temperatures the erosion rate remains fairly constant during the removal of the entire 380 nm film. Only small fluctuations of ±10% of the data points are observed, which is likely to be induced by the surface roughness calibration and ion beam current fluctuations. The sputter yield volume ranges from 200 to 275 nm^3/impact for a 40-keV C_{60}^+ ion beam, in agreement with previously reported values.[3,34]

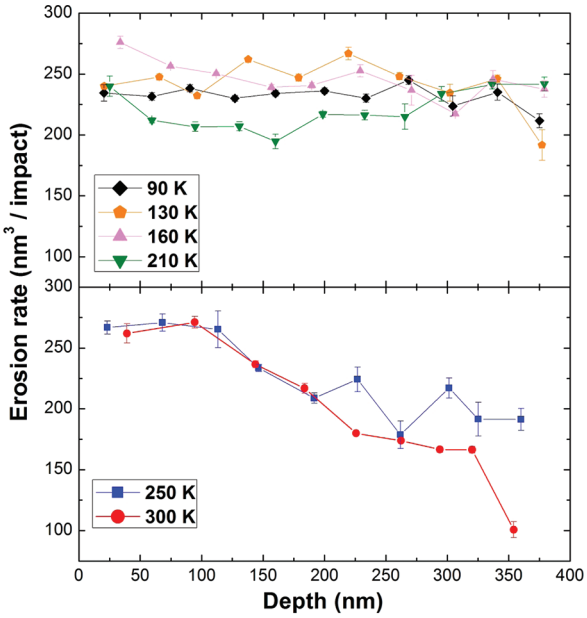

Figure 6. Erosion rate as a function of eroded depth during bombardment of the Irganox 1010/3114 Δ-layer film at 90, 130, 160, and 210 K (top panel) and 250 and 300 K (lower panel). All six wedge craters were created by a 40-keV C_{60}^+ ion beam impinging at 40° with respect to the surface normal.

The second group consists of the experiments performed at 250 and 300 K. These data are plotted in the lower panel of Figure 6. At 250 K, the erosion rate decays to ∼70% of the initial value and starts to fluctuate, while at 300 K it continues to decay throughout the erosion of the rest of the organic film, decaying to about 60% of the original surface value. The last data point at 350 nm depth is only 30% of the original surface value, a finding which might be related to the fact that at this temperature the interface between the Irganox film and the Si substrate appears significantly broadened. Therefore, the data plotted at 350 nm (which was averaged over the depth interval of 340−360 nm) depth might already be influenced by the strong sputter yield reduction at this interface which is caused by the low Si sputter yield.

Interestingly, the decay of the erosion rate at 250 and 300 K begins quite abruptly at ∼100 nm depth. At this point, we can only speculate about the cause of this effect. From the observed temperature dependence, it is clear that a thermally activated process must exist that enables (not prevents!) the yield decay. At present, it is not clear whether or how this threshold value depends upon the thickness of the organic overlayer. For the 400 nm Irganox film investigated here, the threshold temperature for this process to influence the erosion dynamics is somewhere between 210 and 250 K. Reducing the temperature further below this threshold does not lead to any further improvement of the depth profiles. The buildup of roughness suggests that patches exhibiting different sputter yield develop at the surface. Areas with higher sputter yield are being eroded faster, leading to an instability of the surface topography. The fact that the average erosion rate decreases suggests that the sputter yield of these patches must be lowered with respect to the pristine surface. One possible process that may trigger this behavior is that carbon atoms implanted from the projectiles diffuse and nucleate, forming amorphous or graphitic carbon clusters which are known to exhibit low sputter yield under C_{60} bombardment.[38]

dx.doi.org/10.1021/ac2032589 | Anal. Chem. 2012, 84, 3981−3989

It is also interesting to note that the drop of the erosion rate at the beginning of the depth profile appears more pronounced in Figure 2 than in Figure 6. In principle, we consider the wedge data more reliable, since it is solely based on a geometric measurement without any further assumptions. This means that the average erosion rate between the surface and the first Δ-layer as plotted in Figure 2 must be overestimated. In fact, it is a common observation in Δ-layer depth profiling that the peak of the SIMS signal representing the layer is observed at lower ion fluence than needed to erode to the actual depth of the layer. Such a "differential shift" has been observed in SIMS Δ-layer depth profiling of inorganic target many times.[39] It can be quantitatively understood in terms of the statistical nature of the sputtering process[40,41] and appears to be mainly caused by ion beam induced interlayer mixing. For the system of Δ-layers studied here, it would lead to an overestimation of the average erosion rate from the surface to the first Δ-layer. Since the shift remains the same for all following layers, the fluence interval between the deeper layers then correctly reflects the actual distance between those layers. The data in Figure 2 reveal that the shift is largest at room temperature, suggesting that the mixing depth is temperature dependent and decreases with decreasing sample temperature. The model calculations[40] also suggest that the observed depth resolution should be much less affected by the mixing depth than the differential shift, a notion which is consistent with our finding of a constant fwhm of the first Δ-layer in Figure 1.

CONCLUSION

The present work expands upon the investigation of temperature effects previously observed on an Irganox organic Δ-layer system by adding new information obtained at different sample temperatures. By combining conventional depth profiling and wedge-crater beveling, the effect of temperature on fundamental factors such as surface roughness, erosion rate, depth resolution, and molecular signal intensity as well as their variation as a function of eroded depth are unraveled for the first time. We find the following key observations: (1) The estimation of average erosion rates from the ion fluence needed to reach the different Δ-layers is misleading due to the "differential shift" of the SIMS response peaks. Reliable data on depth dependent erosion rates can, however, be obtained using the wedge beveling strategy. (2) The degradation of depth resolution is linked to a decay of the average erosion rate. This decay is always accompanied by a buildup of surface roughness, suggesting that both phenomena are caused by the same process. For the system studied here, this process is temperature dependent and becomes suppressed at temperatures below a threshold value somewhere between 210 and 250 K. Above this threshold, the process becomes more efficient, while at lower temperature no further improvement of the depth profile is observed. (3) The erosion rate decay/surface roughness buildup starts only after erosion of a certain depth (here: 100−150 nm) and must therefore be related to a cumulative effect. Under conditions where this effect is inhibited, the observed depth resolution does not depend upon the sample temperature. (4) The measured molecular secondary ion signal intensity degrades with increasing eroded depth in a way that is clearly temperature dependent and inhibited for sample temperatures below 250 K. The signal degradation is more pronounced for the larger molecular fragments, indicating that it is caused by accumulating chemical damage.

It is striking that signal degradation is also observed during erosion of the first 100 nm, where neither the sputter yield nor the surface roughness appears to change and the depth resolution remains constant. Therefore, this signal reduction cannot be attributed to a sputter yield decay alone as predicted by the erosion dynamics model. Apparently, the damage accumulated in this regime still has no effect on the erosion rate and surface topography. Another possible explanation is that the signal reduction is caused by a changing ionization probability of the desorbed fragments. At present, however, it is not clear why such a process would lead to a stronger decay for larger fragments. Since the process is inhibited by sample cooling, it must also be fused by a thermally activated mechanism. Evidently, a certain threshold damage must be reached in order to trigger the erosion rate and topography changes. In light of the discussion above, one could envision that defects introduced by the projectile impact gradually build up in concentration and diffuse with a temperature controlled mobility, until at some point a critical concentration is reached and nucleation of defect clusters large enough to influence the erosion rate sets in. Although this notion would be consistent with the observed temperature dependence of erosion rate and surface topography, it is not sufficient to explain the signal decay observed during the first 100 nm of the depth profile at high temperatures. Here, further studies involving, for instance, postionization of sputtered neutral fragments are needed in order to clarify the cause of the observed effect.

AUTHOR INFORMATION

Corresponding Author

*E-mail: nxw@psu.edu.

Notes

The authors declare no competing financial interest.

ACKNOWLEDGMENTS

Financial support from the National Institute of Health under Grant No. 2R01 EB002016-18, the National Science Foundation under Grant No. CHE-0908226, and the Department of Energy Grant No. DE-FG02-06ER15803 is acknowledged. The authors are grateful to Alex Shard of the National Physical Laboratory for providing the Δ-layer sample.

REFERENCES

(1) Sun, S.; Wucher, A.; Szakal, C.; Winograd, N. *Appl. Phys. Lett.* **2004**, *84*, 5177.
(2) Wagner, M. S. *Anal. Chem.* **2005**, *77*, 911.
(3) Shard, A. G.; Green, F. M.; Brewer, P. J.; Seah, M. P.; Gilmore, I. S. *J. Phys. Chem. B* **2008**, *112*, 2596.
(4) Mahoney, C. M.; Fahey, A. J.; Gillen, G. *Anal. Chem.* **2007**, *79*, 828.
(5) Zheng, L. L.; Wucher, A.; Winograd, N. *Anal. Chem.* **2008**, *80*, 7363.
(6) Ninomiya, S.; Ichiki, K.; Yamada, H.; Nakata, Y.; Seki, T.; Aoki, T.; Matsuo, J. *Rapid Commun. Mass Spectrom.* **2009**, *23*, 3264.
(7) Lee, J. L. S.; Ninomiya, S.; Matsuo, J.; Gilmore, I. S.; Seah, M. P.; Shard, A. G. *Anal. Chem.* **2010**, *82*, 98.
(8) Sjovall, P.; Rading, D.; Ray, S.; Yang, L.; Shard, A. G. *J. Phys. Chem. B* **2010**, *114*, 769.
(9) Lu, C. Y.; Wucher, A.; Winograd, N. *Anal. Chem.* **2011**, *83*, 351.
(10) Shard, A. G.; Foster, R.; Gilmore, I. S.; Lee, J. L. S.; Ray, S.; Yang, L. *Surf. Interface Anal.* **2011**, *43*, 510.
(11) Cheng, J.; Winograd, N. *Anal. Chem.* **2005**, *77*, 3651.
(12) Fletcher, J. S.; Conlan, X. A.; Lockyer, N. P.; Vickerman, J. C. *Appl. Surf. Sci.* **2006**, *252*, 6513.

(13) Gillen, G.; Roberson, S. *Rapid Commun. Mass. Spectrom.* **1998**, *12*, 1303.
(14) Wagner, M. S.; Gillen, G. *Appl. Surf. Sci.* **2004**, *231−2*, 169.
(15) Mahoney, C. M.; Roberson, S. V.; Gillen, G. *Anal. Chem.* **2004**, *76*, 3199.
(16) Fletcher, J. S.; Lockyer, N. P.; Vickerman, J. C. *Mass Spectrom. Rev.* **2011**, *30*, 142.
(17) Rabbani, S.; Barber, A. M.; Fletcher, J. S.; Lockyer, N. P.; Vickerman, J. C. *Anal. Chem.* **2011**, *83*, 3793.
(18) Fletcher, J. S.; Lockyer, N. P.; Vaidyanathan, S.; Vickerman, J. C. *Anal. Chem.* **2007**, *79*, 2199.
(19) Nygren, H.; Hagenhoff, B.; Malmberg, P.; Nilsson, M.; Richter, K. *Microsc. Res. Tech.* **2007**, *70*, 969.
(20) Zheng, L. L.; Wucher, A.; Winograd, N. *Appl. Surf. Sci.* **2008**, *255*, 816.
(21) Wucher, A.; Cheng, J.; Winograd, N. *Appl. Surf. Sci.* **2008**, *255*, 959.
(22) Fletcher, J. S.; Vickerman, J. C. *Anal. Bioanal. Chem.* **2010**, *396*, 85.
(23) Wucher, A.; Cheng, J.; Zheng, L.; Winograd, N. *Anal. Bioanal. Chem.* **2009**, *393*, 1835.
(24) Matsuo, J.; Ninomiya, S.; Nakata, Y.; Honda, Y.; Ichiki, K.; Seki, T.; Aoki, T. *Appl. Surf. Sci.* **2008**, *255*, 1235.
(25) Ichiki, H.; Orihara, K.; Hamasaki, S.; Ishida, S.; Oketani, N.; Iriki, Y.; Ninomiya, Y.; Okui, H.; Kuwahata, S.; Fujita, S.; Matsushita, T.; Yoshifuku, S.; Oba, R.; Hirai, H.; Nagata, K.; Tei, C. *J. Cardiol.* **2009**, *53*, 127.
(26) Kozole, J.; Willingham, D.; Winograd, N. *Appl. Surf. Sci.* **2008**, *255*, 1068.
(27) Chandra, S.; Morrison, G. H. *Biol. Cell* **1992**, *74*, 31.
(28) Colliver, T. L.; Brummel, C. L.; Pacholski, M. L.; Swanek, F. D.; Ewing, A. G.; Winograd, N. *Anal. Chem.* **1997**, *69*, 2225.
(29) Ostrowski, S. G.; Van Bell, C. T.; Winograd, N.; Ewing, A. G. *Science* **2004**, *305*, 71.
(30) Mahoney, C. M.; Fahey, A. J.; Gillen, G.; Xu, C.; Batteas, J. D. *Appl. Surf. Sci.* **2006**, *252*, 6502.
(31) Mao, D.; Lu, C.; Winograd, N.; Wucher, A. *Anal. Chem.* **2011**, *83*, 6410.
(32) Dowsett, M. G.; Rowlands, G.; Allen, P. N.; Barlow, R. D. *Surf. Interface Anal.* **1994**, *21*, 310.
(33) Braun, R. M.; Blenkinsopp, P.; Mullock, S. J.; Corlett, C.; Willey, K. F.; Vickerman, J. C.; Winograd, N. *Rapid Commun. Mass. Spectrom.* **1998**, *12*, 1246.
(34) Mao, D.; Wucher, A.; Winograd, N. *Anal. Chem.* **2010**, *82*, 57.
(35) Cheng, J.; Wucher, A.; Winograd, N. *J. Phys. Chem. B* **2006**, *110*, 8329.
(36) Wucher, A. *Surf. Interface Anal.* **2008**, *40*, 1545.
(37) Kozole, J.; Wucher, A.; Winograd, N. *Anal. Chem.* **2008**, *80*, 5293.
(38) Krantzman, K. D.; Webbb, R. P.; Garrison, B. J. *Appl. Surf. Sci.* **2008**, *255*, 837.
(39) Dowsett, M. G.; Barlow, R. D.; Allen, P. N. *J. Vac. Sci. Technol., B* **1994**, *12*, 186.
(40) Wucher, A.; K., K. D.; Lu, C.; Winograd, N. *Surf. Interface Anal.* **2012**, in press.
(41) Paruch, R. J.; Postawa, Z.; Wucher, A.; Garrison, B. J. *J. Phys. Chem. C* **2012**, *116*, 1042.